Scripta Materialia 242 (2024) 115917

Contents lists available at ScienceDirect

Scripta Materialia

journal homepage: www.journals.elsevier.com/scripta-materialia

Sc diffusion in HCP high entropy alloys

Sandipan Sen [a,*], Xi Zhang [b], Lukasz Rogal [c], Juliana Schell [d,e], Gerhard Wilde [a], Blazej Grabowski [b], Sergiy V. Divinski [a,*]

[a] Institute of Materials Physics, University of Münster, Wilhelm-Klemm-Str. 10, 48149 Münster, Germany
[b] Institute for Materials Science, University of Stuttgart, 70569 Stuttgart, Germany
[c] Institute of Metallurgy and Materials Science, Polish Academy of Sciences, Krakow, Poland
[d] European Organization for Nuclear Research (CERN), CH-1211, Geneva, Switzerland
[e] Institute for Materials Science and Center for Nanointegration Duisburg-Essen (CENIDE), University of Duisburg-Essen, 45141, Essen, Germany

ARTICLE INFO

Keywords:
Diffusion
High-entropy alloy
AlScHfTiZr
HCP crystalline lattice

ABSTRACT

Sc diffusion in hexagonal close packed $Al_{15}Hf_{25}Sc_{10}Ti_{25}Zr_{25}$ and $Al_5Hf_{25}Sc_{20}Ti_{25}Zr_{25}$ high-entropy alloys is measured using the CERN facility for implantation of the ^{46}Sc isotope. The Sc diffusivity is found to be slower than that of previously measured Ti in both alloys. *Ab initio*-informed calculations are used to quantify the interplay of chemical complexity and local atomic strains. The mean-square atomic displacements are shown to contribute to the observed "anti-sluggish" diffusion behavior in these high-entropy alloys.

The scientific interest in high entropy alloys (HEAs) has been steadily increasing in the past decades [1,2]. Contrary to the standard solute-solvent model of alloy formation, HEAs feature an equiatomic or nearly-equiatomic composition. The majority of the diffusion studies on HEAs have been focused on cubic systems [3–5], see, e.g., Ref. [6] for a recent review. There are only a handful of HEAs that have been reported for hexagonal close packed (HCP) crystal structures [7–9]. Most of these HCP alloys contain lanthanides or actinides, and are thus expensive to synthesize and replicate. An exception is the study of Rogal et al. [10] who developed HCP HEAs with the compositions of $Al_{15}Hf_{25}Sc_{10}Ti_{25}Zr_{25}$ and $Al_5Hf_{25}Sc_{20}Ti_{25}Zr_{25}$.

Tracer diffusion of Ti [11] and Zn (as an Al-substitute) [12] was measured recently in these HEAs revealing an unexpected "anti-sluggish" diffusion behavior of Ti in clear contradiction to the long-standing paradigm of "sluggish diffusion" postulated as a core effect for HEAs [13,14]. The reported anti-sluggish behavior was quantified by a dramatic increase of the diffusivity with respect to the diffusivities in the corresponding unary systems. Considering the chemical complexity of HEAs, one may expect a certain diffusion retardation based on a simple energy barrier reasoning [15]. One may argue that severe lattice distortions influence the vibrational contribution to the diffusion rates in a way that Ti diffusion in the HCP high-entropy alloys becomes faster than in unary HCP metals [11]. The importance of lattice vibrations (and of the related excess entropy contribution over the configurational term) for stability and properties of HEAs has been indeed recognized recently [16,17].

Two types of lattice distortions can generally be considered: (i) element-averaged lattice distortions (δ) estimated from the atomic radii incompatibility [18], or (ii) element-specific lattice strains represented by mean-square atomic displacements (MSAD) determined, e.g., using density-functional-theory (DFT) calculations [11]. Comparing the two compositions of the HCP HEAs, $Al_{15}Hf_{25}Sc_{10}Ti_{25}Zr_{25}$ and $Al_5Hf_{25}Sc_{20}Ti_{25}Zr_{25}$ denoted as 15Al and 5Al in this paper, the relative trends of these two types of lattice distortions are the same for Ti atoms, i.e., $\delta_{15Al} > \delta_{5Al}$ and $MSAD^{Ti}_{15Al} > MSAD^{Ti}_{5Al}$ [11]. This trend is also obeyed by the Ti diffusivities, i.e., $D^{Ti}_{15Al} > D^{Ti}_{5Al}$ [11].

On the contrary, for the lattice distortions of Sc atoms, an opposite relation was found to hold, i.e., $MSAD^{Sc}_{15Al} < MSAD^{Sc}_{5Al}$ [11]. Obviously, the lattice-averaged lattice distortion relationship between the two alloys remains the same, i.e., $\delta_{15Al} > \delta_{5Al}$. Thus, whereas for Ti the trends for the element-averaged lattice distortions (δ) and element specific MSAD are the same for 5Al and 15Al, for Sc these trends are opposite. In the present study, we measure Sc self-diffusion in these HCP HEAs and shed further light onto the interplay of lattice distortions and chemical heterogeneity in relation to diffusion phenomena in HEAs.

The synthesis, sample preparation and heat treatments are identical to the ones described in our previous publications [19,11,12]. The results of microstructure, phase and chemical homogeneity investigations of the alloys via X-ray diffraction (XRD), electron back-scatter diffrac-

* Corresponding authors.
E-mail addresses: ssen@wwu.de (S. Sen), divin@wwu.de (S.V. Divinski).

https://doi.org/10.1016/j.scriptamat.2023.115917
Received 17 June 2023; Received in revised form 23 October 2023; Accepted 30 November 2023
Available online 14 December 2023

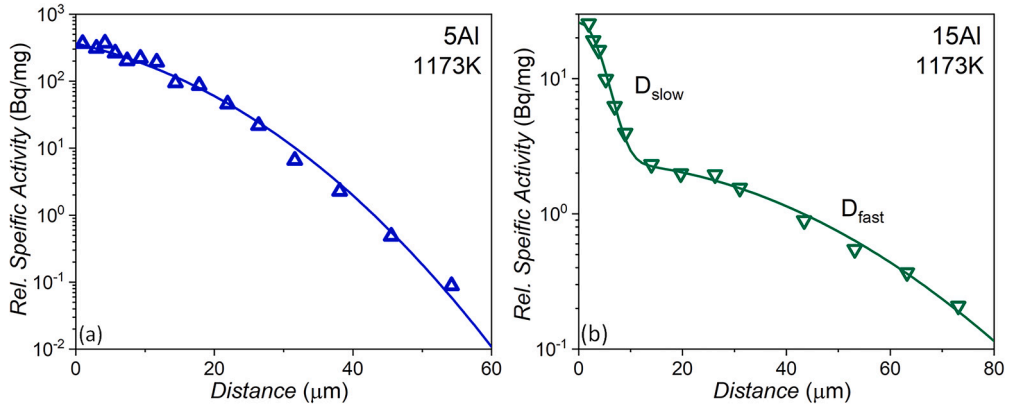

Fig. 1. Penetration profiles for ^{46}Sc diffusion in 5Al (a) and 15Al (b) HEAs at 1173 K.

Table 1
Annealing temperatures T and times t, and the determined volume diffusion coefficients D for ^{46}Sc diffusion in the two quinary HCP HEAs. The estimated uncertainties of the diffusion coefficients do not exceed 20%.

Alloy	T (K)	t (10^4 s)	D_{slow} (m^2/s)	D_{fast} (m^2/s)
5Al	973	163.3	1.65×10^{-18}	–
	1173	7.02	1.47×10^{-15}	–
	1373	0.36	5.65×10^{-13}	–
15Al	1073	43.2	9.54×10^{-18}	2.19×10^{-16}
	1173	7.02	1.45×10^{-16}	7.67×10^{-15}
	1373	0.36	5.49×10^{-14}	1.04×10^{-12}

tion (EBSD) and X-ray dispersive spectroscopy measurements were also reported [19,11]. The grain size in both alloys exceeded 200 μm [19].

Discs of the two alloys, with mirror-like surface finishes, were taken to the Isotope-Separator-On-Line-DEvice (ISOLDE) at Conseil Européen pour la Recherche Nucléaire (CERN) where the ^{46}Sc isotope was generated by bombardment of a Ta target with protons. The generated ^{46}Sc beam was focused on the sample surfaces creating an implantation profile with depths of a few tens of nanometer.

The implanted samples were transported to the radiotracer laboratory at the Institute of Materials Physics, University of Münster, Germany; and subjected to specific diffusion annealing treatments, as listed in Table 1. The samples were sectioned parallel to the surface utilizing a high-precision mechanical grinding device. The thickness of each removed section was obtained by measuring the weight loss of the samples after each sectioning step using a Sartorius 2002 MP1 microbalance.

The specific activity of each section was measured by a NaI γ-detector equipped with a 16K multi-channel analyzer. The intensities of two ^{46}Sc γ-peaks at 889.3 keV and 1120.6 keV were added together to increase the signal-to-background ratio.

The penetration profiles were obtained by plotting the relative specific activity of each section (which is proportional to the ^{46}Sc concentration) vs. the section depth. As an example, the penetration profiles measured at 1173 K for 5Al and 15Al alloys are shown in Fig. 1(a, b), respectively. The penetration profiles at the other temperatures for both alloys are of a similarly high quality.

The penetration profiles for 5Al (Fig. 1(a)) follow the instantaneous source solution of the diffusion problem,

$$C(x,t) = \frac{M}{\sqrt{\pi D t}} \exp\left(-\frac{x^2}{4Dt}\right), \tag{1}$$

where M is the initial amount of implanted tracer, D is the diffusion coefficient, t is the annealing time and $C(x,t)$ is the concentration of the tracer at a depth x after time t. When plotted on an absolute inverse temperature scale, the diffusivities follow an Arrhenius-type temperature dependence (Fig. 3(a)).

For the same annealing times and temperatures, the penetration profiles for the 15Al alloy consist of two branches both of which can be separately fitted with Eq. (1) as shown in Fig. 1(b). This is in obvious contrast to 5Al which exhibits only one branch fitted according to Eq. (1) for comparable diffusion depths of 50–70 μm, see Fig. 1(a). Note that in all cases the penetration profiles were followed until the background activity was reached, which corresponds to about 0.1 Bq/mg for the present conditions. Note as well that only one branch was consistently observed for both Ti [11] and Zn [12] diffusion in these alloys which indicates a negligible diffusion anisotropy for these elements. It seems that Sc diffusion in 15Al reveals a significant anisotropy, similar to that of Co [19].

The two branches in 15Al are formally termed as relatively "slow" (the steeper, near-surface) and "fast" (the deeper, shallower one) branches, just to reflect their relative diffusion rates. In view of the HCP structure, an anisotropy of diffusion can be expected [20] with different depths of tracer penetration in grains oriented differently in a polycrystalline material. The present alloys are the same as in our previous work on Co diffusion [19] where coarse-grained microstructure with two main texture components with an inclination, Θ, of about 22° and 74° of the c axis with respect to the sample surface [19] was detected. Thus, the principal diffusivities along ($D_{\parallel}$) and perpendicular ($D_{\perp}$) to the c axis can be determined using

$$D_i = D_{\parallel}\cos^2\Theta_i + D_{\perp}\sin^2\Theta_i, \tag{2}$$

from the measured diffusivities D_i, i.e., D_{slow} and D_{fast}, in 15Al. For a detailed explanation of the specific two-step shape of the concentration profiles the reader is referred to our previous paper [19]. The measured diffusivities and the estimated principal diffusion coefficients are plotted as functions of the inverse temperature in Fig. 2(a). Firstly, similar to the 5Al system, the self-diffusion coefficients follow Arrhenius-type temperature dependencies. Secondly, the measured diffusion coefficients (D_{slow} and D_{fast}) are found to only marginally deviate from the principal diffusivities, i.e., $D_{\parallel}$ and $D_{\perp}$. However, since from the experiments on a polycrystalline material it is not possible to unambiguously quantify the measured diffusivities in terms of the principal ones (formally, two solutions of Eq. (2) corresponding to opposite anisotropy ratios are possible), in Fig. 2(a), the diffusion coefficients along the principal directions are named as D_1 and D_2.

To support the experimental result on the diffusion anisotropy from theory, we performed *ab-initio*-informed kinetic Monte Carlo (kMC) simulations to extract the Sc self-diffusivities in the 15Al alloy. The well-known Einstein relation was applied with an adjustment concerning realistic vacancy concentrations,

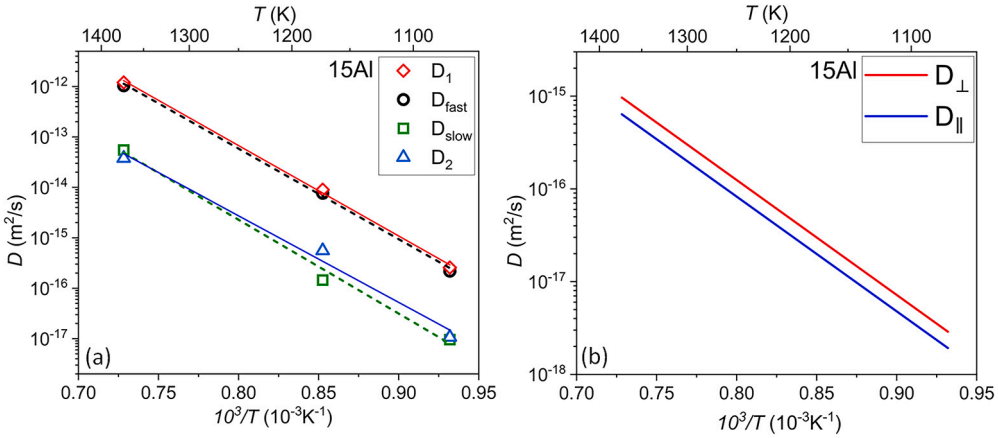

Fig. 2. (a) Arrhenius-type dependence of the Sc diffusivity in the 15Al HEA with the experimentally determined D_{slow} and D_{fast} values (the Arrhenius dependencies are approximated by dashed lines) and the estimated principal D_1 and D_2 values (using Eq. (2), solid lines). (b) Theoretically predicted principal diffusion coefficients of Sc in 15Al (without accounting for entropies of vacancy formation and migration).

$$D_{\perp/\parallel} = \frac{c_V^{eq}}{c_V^{sim}} \cdot \frac{\langle R^2_{\perp/\parallel} \rangle}{2dt}, \tag{3}$$

where $\langle R^2_{\perp/\parallel} \rangle$ is the mean squared displacement of the diffusing atom projected on the corresponding direction, d is the dimension which is 2 for basal-plane diffusion and 1 for diffusion along the c axis, t is the time, and c_V^{eq} and c_V^{sim} refer to the equilibrium vacancy concentration and the vacancy concentration in the simulation box, respectively. The pre-factor, c_V^{eq}/c_V^{sim}, serves to rescale the directly-generated diffusivities to the real diffusivities by assuming that diffusivities are in proportion to the vacancy concentration. The equilibrium vacancy concentrations for the 15Al alloy as reported in Ref. [21] were used. Other technical details related to the kMC simulations are the same as that in Ref. [12].

It is known that self-diffusion in α-Zr [22], α-Ti [23] and α-Hf [24] is faster within the basal plane, i.e., perpendicular to the c axis, with the $D_\parallel/D_\perp$ ratio being 0.6, 0.5 and 0.65 respectively. This behavior is opposite to that for some other HCP elements, e.g., Cd ($D_\parallel/D_\perp = 3.53$ [25]) and Zn ($D_\parallel/D_\perp = 3.57$ [26]).

One may expect that the anisotropy of self-diffusion in the present HCP HEAs is qualitatively similar to that in α-Zr/α-Ti/α-Hf. Indeed, our DFT-informed calculations predict a faster Sc diffusivity within the basal plane with respect to that along the c axis in the 15Al alloy, Fig. 2(b). It has to be noted that these diffusivities were calculated without consideration of the vibrational entropy for both vacancy formation and migration. This explains largely the differences in the absolute values of the diffusion coefficients from experiment, Fig. 2(a), and from theoretical prediction, Fig. 2(b). Note that a reasonable assumption of $5k_B$ for the vibrational entropy brings the predicted diffusivities to the same order of magnitude as the experimentally measured values.

Thus, we may safely assume that the determined values of D_1 and D_2 correspond to $D_\perp$ and $D_\parallel$, respectively. Nevertheless, further calculations are required to provide a deeper theoretical understanding of the experimentally measured diffusion anisotropy, which in 15Al is found to be stronger than in pure α-phases mentioned above and $D_\parallel^{Sc}/D_\perp^{Sc} \approx 0.1$ in 15Al, Fig. 2(a). Such calculations could be a focus of another study.

Most likely, a second, faster contribution in the 5Al sample would also be revealed at larger depths and lower activities. However, its reliable determination was hindered by the relatively high background of the used NaI detector. Note that a similar tendency was observed for Co diffusion in these alloys – at temperatures above 973 K – whereas a dominant single "slow" branch was detected for 5Al, two such contributions both "slow" and "fast" branches, were seen for 15Al [19].

Since only the D_{slow} values are available for both alloys, henceforth we compare these diffusivities only. The measured D_{slow} values are plotted against the absolute inverse temperature, T^{-1}, in Fig. 3(a), and against the inverse homologous temperature, T_m/T, in Fig. 3(b) [T_m is the melting point]. The Sc diffusivities are compared to those measured previously for Ti [11]. On either temperature scale, Sc is found to diffuse slower than Ti in both of the alloys at almost all temperatures. However, the most important observation is that in the temperature range of 973 to 1373 K, Sc is faster in 5Al than in 15Al, a tendency which is opposite to that for Ti diffusion, Fig. 3(a). The estimated Arrhenius parameters for Sc diffusion in both alloys are listed in Table 2. Note that these values have to be treated with caution, since the measurements were performed only at three distinct temperatures, though in extended temperature intervals. The uncertainties of the Arrhenius parameters were determined using Monte-Carlo sampling similarly to the "bootstrapping" [27] algorithm.

Table 2
Activation enthalpy, Q, and the pre-factor, D_0, determined for Sc diffusion in the two quinary HCP HEAs.

Alloy	D_0 (m²/s)	Q (kJ/mol)
5Al	$10.6^{+96.1}_{-9.5}$	352 ± 21
15Al	$1.83^{+42.8}_{-1.75}$	357 ± 31

Sc diffusion is found to be consistently slower than that of Ti atoms in both HCP alloys and the difference between the alloys is larger for Sc than Ti, Fig. 3. This behavior may be related to the differences in the chemical compositions of these two alloys. Whereas the Ti amount remains the same, about 25 at.%, the Sc amount drops from 20 at.% to 10 at.% between the 5Al and 15Al alloys. The previous *ab initio* predictions of the migration barriers [21] suggest no obvious differences between the 0 K migration energy distributions for Sc atoms with respect to those for Ti atoms between these two alloys. Though, detailed kMC investigations, in particular including relevant thermal effects, are required to estimate the correlation factors for atom diffusion in these two alloys and this is a task for a separate study.

By mixing multiple elements on the same lattice, both chemical and lattice distortions become relevant for vacancy migration in terms of potential energy fluctuations (PEFs). In line with this reasoning, PEFs were formulated as a combination of chemical and averaged elastic distortions as described in Ref. [18]. These equations have been included in the supplementary material for convenience.

Since Al does not crystallize on the HCP lattice, there are no experimental data for HCP Al and the atomic radius of the Al atom in a (hypothetical) HCP lattice needs to be calculated. In order to compare the data from the same source, the atomic radii of all the elements were

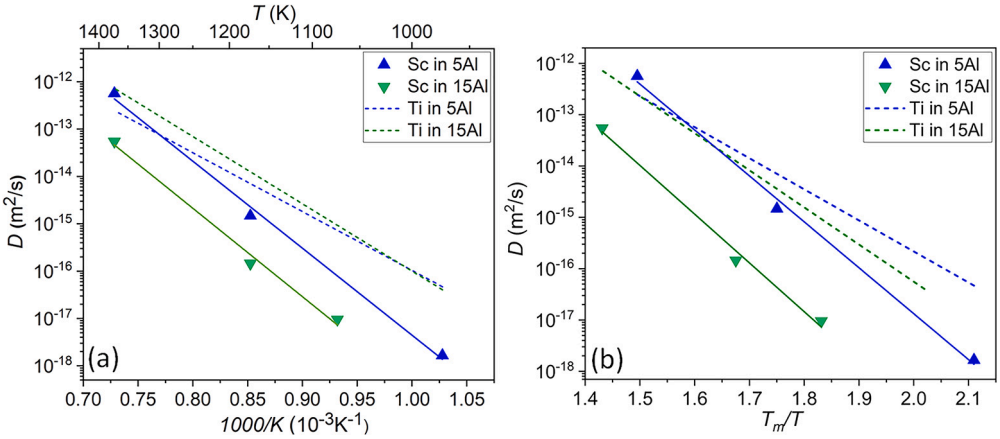

Fig. 3. Temperature dependence of ^{46}Sc diffusion in 5Al and 15Al plotted on the (a) inverse temperature scale and (b) inverse homologous temperature scale. The dashed lines represent the Ti self-diffusion rates measured by Sen et al. [11].

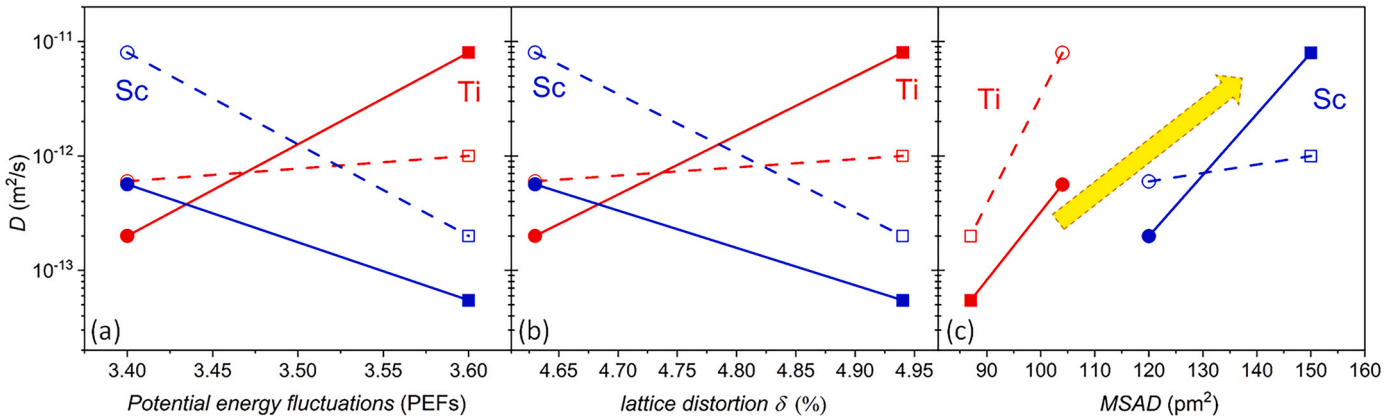

Fig. 4. Diffusion coefficients of Sc (blue) and Ti (red) as function of (a) PEFs, (b) lattice distortions δ and (c) MSAD in HCP HEAs. The data are plotted for $T = 1373$ K (solid lines, filled symbols) and $T = 0.75\,T_m$ (dashed lines, open symbols) for both 5Al (squares) and 15Al (circles) alloys. The yellow arrow sketches the anticipated trend provided by the element-specific MSAD values. (For interpretation of the colors in the figure(s), the reader is referred to the web version of this article.)

determined by DFT calculations. The details of the calculations were reported in our previous work [11].

Mean-square atomic displacements represent a further parameter which can be relevant for the understanding of vacancy-mediated diffusion in HEAs, especially by analyzing the element's diffusion rates determined by dedicated tracer measurements. DFT calculations were used for this aim, as it was reported in Ref. [11].

Correlations between the calculated PEFs, averaged lattice distortions δ, element-specific MSADs, and the diffusion coefficients are examined in Fig. 4. It is seen that PEFs and δ dependencies do not provide specific global trends. In fact, while D^{Ti} increases with increasing PEFs and δ values, the Sc diffusion coefficients D^{Sc} decrease, Fig. 4(a) and (b). On the contrary, the determined tracer diffusion coefficients reveal systematic trends when plotted against the MSAD values as seen in Fig. 4(c), yellow arrow. In fact, the same trend for both Ti and Sc is clearly seen. It is important to note that the tracer diffusion coefficients and MSAD reveal a correlation, but no direct dependence of the element diffusion coefficients against MSAD can be suggested. Nevertheless, MSADs seem to be the relevant parameters to quantify the diffusion behavior in HEAs and they perform at least better as PEFs or lattice distortions δ.

The importance of MSAD for the diffusion behavior in HEAs can be illustrated by accounting for the variations of the diffusion jump barriers, E_b^{k-l}, site energies, E_s^k, and the diffusion jump lengths, λ^{k-l}. Here the indices k and l enumerate successive sites and corresponding saddle point positions of a vacancy during its diffusion walk through the lattice. Tsai et al. [15], had originally related the anticipated retardation of diffusion in FCC CoCrFeMnNi HEA to the variation of lattice PEFs caused by local variations of the site energies, E_s^k, resulting from a random distribution of unlike atoms on the same lattice. This concept is schematically shown in Fig. 5(a) referring to an artificial mono-atomic lattice. This model, however, does not account for the element-specific lattice distortions, which in fact cannot be neglected as the present results unambiguously demonstrate.

In Fig. 5(b), the effects of element specific lattice distortions (in fact, MSADs) are shown in combination with a variation of local jump barriers (green curve). An energy profile for a perfect mono-atomic lattice is drawn for comparison (black line). Due to mixing of unlike atoms on a common lattice (as is the case of HEAs), energy barriers, site energies, and the jump lengths vary along the vacancy migration path. Since the jump probability from a site k to a neighboring site l is defined by the total free energy barrier, $\Delta G_b^{k-l} - \Delta G_s^k$, both enthalpic (PEFs) and entropic (vibration frequencies of atoms at different configurations) terms determine the diffusion rates.

The "sluggish" diffusion concept, based on local variations of the lattice potential energy landscape [15], was found to be partially applicable for FCC HEAs [28], but disagrees with the observed diffusion behavior in BCC [5] or HCP [11] HEAs. The lattice distortions were suggested to play an important role in describing the diffusion behavior of HEAs [11]. In accord with these predictions, the MSADs reported for FCC HEAs are significantly lower than those for HCP HEAs [11,29,30] which would explain why lattice distortions play a greater effect in HCP HEAs than the FCC HEAs. Along a similar line of discussion, Dong et al. [31], showed that in BCC refractory HEAs and their subsystems, lattice

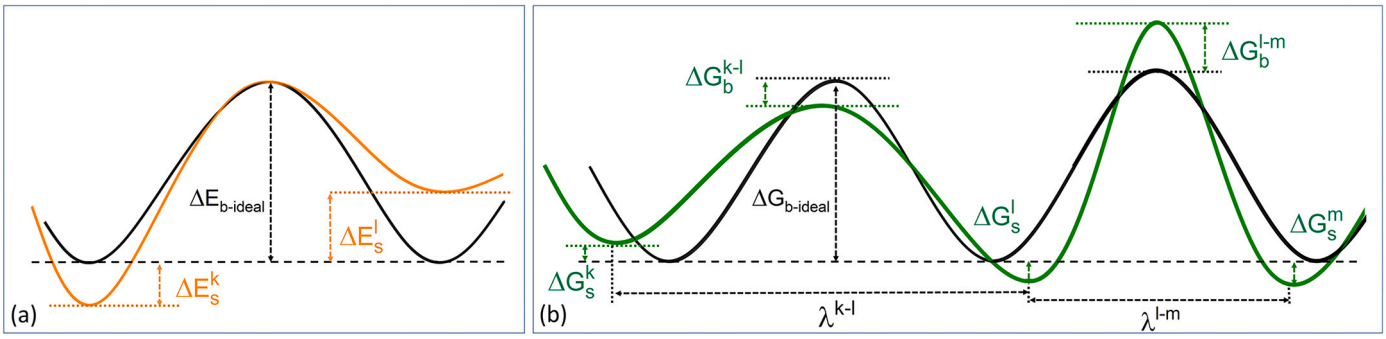

Fig. 5. Schematic of (a) the potential energy landscape for a migrating vacancy with varying site energies E_s^k and (b) the free energy landscape with variation of all relevant parameters, ΔG_s^k, ΔG_b^{k-l}, and λ^{k-l}. The changes of the parameters with respect to those for an ideal mono-atomic lattice (black line) are indicated. The super-scripts (k, l, m, ...) index successive vacancy positions. Scheme (a) is drawn following Ref. [15].

distortions rather than chemical complexity play a larger role in influencing electrical resistivity, as compared to the 3*d* transition metal FCC HEAs.

To summarize the present work, diffusion of Sc in the two HCP HEAs $Al_5Hf_{25}Sc_{20}Ti_{25}Zr_{25}$ and $Al_{15}Hf_{25}Sc_{10}Ti_{25}Zr_{25}$ has been investigated and, within the temperature interval of experiments, $D^{Sc}_{15Al} < D^{Sc}_{5Al}$ has been obtained. This relationship for Sc is opposite to that observed previously for Ti, $D^{Ti}_{15Al} > D^{Ti}_{5Al}$ [11]. The observed behavior has been explained in terms of element specific lattice distortions. These findings call for consistent calculations of the free energy barriers of vacancy migration in HEAs in future studies.

Declaration of competing interest

The authors declare that they have no known competing financial interests or personal relationships that could have appeared to influence the work reported in this paper.

Acknowledgement

Financial support from the Deutsche Forschungsgemeinschaft (DFG) via the research projects DI 1419/17-1, DI 1419/24-1, GR 3716/5-1, and ZH 1218/1-1 is gratefully acknowledged. X.Z. and B.G. acknowledge the support by the State of Baden-Württemberg through bwHPC and the German Research Foundation (DFG) through grant No. INST 40/575-1 FUGG (JUSTUS 2 cluster) and by the Stuttgart Center for Simulation Science (SimTech). J.S. acknowledges the financial support received from the Federal Ministry of Education and Research (BMBF) through grants 05K16PGA and 05K22PGA. We also acknowledge the support of all the technical teams at ISOLDE for their excellent work in delivering high-quality beams for diffusion measurements. We acknowledge the support of the European Union's Horizon 2020 Framework research and innovation program under grant agreement No. 654002 (ENSAR2) and grant agreement No. 865855 (Materials 4.0).

Appendix A. Supplementary material

Supplementary material related to this article can be found online at https://doi.org/10.1016/j.scriptamat.2023.115917.

References

[1] D.B. Miracle, O.N. Senkov, Acta Mater. 122 (2017) 448–511.
[2] E.P. George, D. Raabe, R.O. Ritchie, Nat. Rev. Mater. 4 (2019) 515–534.
[3] M. Vaidya, S. Trubel, B.S. Murty, G. Wilde, S.V. Divinski, J. Alloys Compd. 688 (2016) 994–1001.
[4] D. Gaertner, L. Belkacemi, V.A. Esin, F. Jomard, A.A. Fedotov, J. Schell, J.V. Osinskaya, A.V. Pokoev, C. Duhamel, A. Paul, S.V. Divinski, Diffus. Found. 29 (2021) 31–73.
[5] J. Zhang, C. Gadelmeier, S. Sen, R. Wang, X. Zhang, Y. Zhong, U. Glatzel, B. Grabowski, G. Wilde, S.V. Divinski, Acta Mater. 233 (2022) 117970.
[6] A. Dash, A. Paul, S. Sen, S.V. Divinski, J. Kundin, I. Steinbach, B. Grabowski, X. Zhang, Annu. Rev. Mater. Res. 52 (2022) 383–409.
[7] M.C. Gao, B. Zhang, S.M. Guo, J.A. Qiao, J.W. Hawk, Metall. Mater. Trans. A 47 (2016) 3322–3332.
[8] Y.J. Zhao, J.W. Qiao, S.G. Ma, M.C. Gao, H.J. Yang, M.W. Chen, Y. Zhang, Mater. Des. 96 (2016) 10–15.
[9] R. Soler, A. Evirgen, M. Yao, C. Kirchlechner, F. Stein, M. Feuerbacher, D. Raabe, G. Dehm, Acta Mater. 156 (2018) 86–96.
[10] L. Rogal, P. Bobrowski, F. Körmann, S.V. Divinski, F. Stein, B. Grabowski, Sci. Rep. 7 (2017) 2209.
[11] S. Sen, X. Zhang, L. Rogal, G. Wilde, B. Grabowski, S.V. Divinski, Scr. Mater. 224 (2023) 115117.
[12] S. Sen, X. Zhang, L. Rogal, G. Wilde, B. Grabowski, S.V. Divinski, Scr. Mater. 229 (2023) 115376.
[13] K.H. Cheng, C.H. Lai, S.J. Lin, J.W. Yeh, Ann. Chim. Sci. Mater. 31 (2006) 723–736.
[14] B.S. Murty, J.W. Yeh, S. Ranganathan, Butterworth-Heinemann, Boston, 2014.
[15] K.-Y. Tsai, M.-H. Tsai, J.-W. Yeh, Acta Mater. 61 (13) (2013) 4887–4897.
[16] J. Wang, J. Li, Q. Wang, J. Wang, Z. Wang, C.T. Liu, Scr. Mater. 168 (2019) 19–22.
[17] M. Esters, C. Oses, D. Hicks, M.J. Mehl, M. Jahnatek, M.D. Hossain, J.P. Maria, D.W. Brenner, C. Toher, S. Curtarolo, Nat. Commun. 12 (2021) 5747.
[18] Q. He, Y. Ye, Y. Yang, J. Appl. Phys. 120 (15) (2016) 154902.
[19] M. Vaidya, S. Sen, X. Zhang, L. Frommeyer, L. Rogal, S. Sankaran, B. Grabowski, G. Wilde, S.V. Divinski, Acta Mater. 196 (2020) 220–230.
[20] H. Mehrer, Diffusion in Solid Matter, Springer, Heidelberg, 2007.
[21] X. Zhang, S.V. Divinski, B. Grabowski, Acta Mater. 227 (2022) 117677.
[22] G.M. Hood, H. Zou, R.J. Schultz, N. Matsuura, J.A. Roy, J. Jackman, Defect Diffus. Forum 143 (1997) 49–54.
[23] M. Köppers, Chr Herzig, M. Friesel, Y. Mishin, Acta Mater. 45 (10) (1997) 4181–4191.
[24] C. Herzig, S. Divinski, Y. Mishin, Metall. Mater. Trans. A 33 (2002) 765–775.
[25] C. Mao, Phys. Rev. B 5 (12) (1972) 4693.
[26] N.L. Peterson, S.J. Rothman, Phys. Rev. 163 (3) (1967) 645.
[27] B. Efron, R. Tibshirani, An Introduction to the Bootstrap, Chapman & Hall/CRC, Boca Raton, FL, 1993.
[28] J. Kottke, D. Utt, M. Laurent-Brocq, A. Fareed, D. Gaertner, L. Perriere, L. Rogal, A. Stukowski, K. Albe, S.V. Divinski, G. Wilde, Acta Mater. 194 (2020) 236–248.
[29] N.L. Okamoto, K. Yuge, K. Tanaka, H. Inui, E.P. George, AIP Adv. 6 (12) (2016) 125008.
[30] M. Masataka, S. Kazuki, A. Hideki, Comput. Mater. Sci. 170 (2019) 109163.
[31] Y. Dong, S. Mu, X. Guo, J. Han, J. Duan, N. Jia, Y. Xue, K. Jin, Scr. Mater. 231 (2023) 115464.